Scattering of High Frequency Waves in the Presence of Whistler Wave Turbulence in the Ionosphere

V. Sotnikov
Air Force Research Laboratory, Wright Patterson AFB, OH 45433, USA

N. Gershenzon, N. Zechar, R. Schueler
Riverside Research Institute, Beavercreek, OH 45431, USA

T. Kim
Asian Office of Aerospace Research and Development, Tokyo 106-0032, Japan

Abstract

The propagation and non-linear interaction of high frequency (HF) electromagnetic (EM) waves through an ionospheric F-layer region with developed whistler wave turbulence is investigated using theory and simulation. In order to analyze HF wave scattering and the non-linear generation of sideband emissions in a spatially and time varying ionospheric plasma, finite difference time domain (FDTD) code was employed. An important feature of this code takes into account spatially and time varying electron plasma densities, which describe turbulent pulsations excited in the ionosphere. It is worth noting, the non-linear generation of sideband emissions can only be observed when resonance conditions in frequency and wave vector domains are simultaneously imposed on interacting HF and whistler waves. Using this FDTD code we present results on the generation of HF sidebands due to HF wave propagation through an ionospheric F-layer region containing whistler wave turbulence.

I. Introduction

Electromagnetic wave propagation through a magnetized ionospheric plasma is an important aspect of long-range radio communications, satellite communications, and radar applications. In the case of a naturally or artificially disturbed ionosphere, electron density irregularities can cause variations in the amplitude and phase of a propagating wave. In particular, these experiments reveal that HF EM pump waves, emitted from the ground to the ionosphere, produce measurable modifications to the plasma along the path of the HF waves.

One of the manifestations of such changes is the generation of very low frequency (VLF) waves which can be detected on the ground. It was also demonstrated that an intensive scattering of HF waves due to the interaction with excited low frequency perturbations can take place. The frequency of the scattered waves can be slightly modified compared to the frequency of the incident wave. This frequency shift is connected between a parametric interaction of HF and VLF waves. Numerus experimental and

theoretical studies related to the HAARP experimental campaigns can be found in the articles [1-12] and references therein.

In our simulations, we examine the possibility of sideband generation due to HF waves propagating through a plasma volume containing VLF waves. Our analysis is based on the studies [17-19] showing sidebands may appear due to nonlinear interaction of finite amplitude waves if certain resonance conditions on frequencies of interacting waves are satisfied. The mechanism of sideband generation is connected with the appearance of induced charges and currents under the action of an incident EM wave. In [19] it was shown that scattering HF waves on ion-acoustic plasma turbulence results in the appearance of sideband emissions above and below that of the source. Here we analyze the interaction of a HF wave and a whistler wave having a frequency close to the electron cyclotron frequency and demonstrate that under certain conditions this interaction leads to the appearance of HF waves with shifted frequencies and wave vectors.

In Section II we will find the necessary requirements for interacting HF and whistler waves to satisfy resonance conditions necessary for efficient excitation of a sideband wave. In Section III, after the required plasma and interacting wave parameters are found we will carry out FDTD simulations using recently developed numerical code. We will analyze the propagation of HF waves through a magnetized plasma perturbed with VLF waves with parameters that satisfy resonance conditions found in the Section II. This will explicitly demonstrate the appearance of the sideband HF waves. The simulations are implemented using full wave propagation code by implementation of FDTD techniques [20] developed for magnetized plasmas [21]. Section IV contains the conclusions.

II. Parametric excitation of sideband HF wave by interaction of whistler and HF waves

The system of equations describing collisionless cold plasma in a magnetic field with first order nonlinear terms arising due to the presence of two HF electromagnetic pump waves are

$$\vec{E} = -\nabla\varphi - \frac{1}{c}\frac{\partial \vec{A}}{\partial t} \tag{1}$$

$$\vec{H} = \nabla \times \vec{A} \tag{2}$$

$$\nabla \cdot \vec{A} = 0 \tag{3}$$

$$\Delta\vec{A} - \frac{1}{c^2}\frac{\partial^2 \vec{A}}{\partial t^2} - \frac{1}{c}\nabla\frac{\partial\varphi}{\partial t} - \frac{4\pi e n_0}{c}\vec{V} = \frac{4\pi e n_{e(1)}}{c}\vec{V}_{(2)} \tag{4}$$

$$\Delta\frac{\partial\varphi}{\partial t}+4\pi en_0\left(\nabla\cdot\vec{V}\right)=-4\pi en_0\left(\nabla\cdot n_{e(1)}\vec{V}_{(2)}\right) \tag{5}$$

$$\frac{\partial V_z}{\partial t}+\frac{e}{m}E_z=-\frac{e}{m_e c}\left[\vec{V}_{(1)}\vec{H}_{(2)}\right]_z-\left(\vec{V}_{(1)}\nabla\right)V_{z(2)} \tag{6}$$

$$\frac{\partial V_x}{\partial t}+\frac{e}{m}E_x+\omega_{He}V_y=-\frac{e}{m_e c}\left[\vec{V}_{(1)}\vec{H}_{(2)}\right]_x-\left[\left(\vec{V}_{(1)}\nabla\right)\vec{V}_{(2)}\right]_x \tag{7}$$

$$\frac{\partial V_y}{\partial t}+\frac{e}{m}E_y+\omega_{He}V_x=-\frac{e}{m_e c}\left[\vec{V}_{(1)}\vec{H}_{(2)}\right]_y-\left[\left(\vec{V}_{(1)}\nabla\right)\vec{V}_{(2)}\right]_y \tag{8}$$

$$\frac{\partial n_e}{\partial t}+\nabla\cdot n_0\vec{V}=-\nabla\cdot\left(n_{e(1)}\vec{V}_{(2)}\right) \tag{9}$$

where $\vec{E}$ and $\vec{H}$ are induced electric and magnetic fields, φ and $\vec{A}$ are electric and magnetic potentials; n_e is the disturbance of electron density, $\vec{V}$ is the velocity of electrons; ω_{He} is the electron cyclotron frequency; e, n_0 , and m_e are the electron charge, background density, and mass, and c is the velocity of light. The right-hand side of equations (4) – (9) are nonlinear terms, which describe the interaction between HF waves and VLF waves, subscripts 1 and 2, respectively. The system of equations (1) - (9) describes both HF and VLF waves.

First, let us suppose the existence of plane monochromatic noted as HF1 wave with frequency ω_{HF1} and wave vector k_{HF1}. Next we suppose a VLF wave with frequency ω_{VLF} and wave number k_{VLF}. The sideband HF2 wave appears if conditions (10) are satisfied:

$$\begin{gathered}\omega_{HF2}=\omega_{HF1}\pm\omega_{VLF}\\ k_{HF2(i)}=k_{HF1(i)}\pm k_{VLF(i)}\,,i=x,y,z\end{gathered} \tag{10}$$

here ω_{HF2} and k_{HF2} are the frequency and wave numbers of sideband HF2 wave. System (1) – (9) without nonlinear terms and for monochromatic wave become a system of linear algebraic equations. Using these equations and conditions (10) one can find the parameters of the HF2 wave from the parameters of VLF wave and HF1 wave.

The angles between the geomagnetic field and HF1 and HF2 waves are θ_1 and θ_2, respectively. Each pair of angles θ_1 and θ_2 requires a specific resonant electron density ($n_{e,res}$) to satisfy conditions (10). We limit our consideration for the case when the electron plasma frequency (ω_{pe}) is larger than the cyclotron

frequency, (ω_{He}). Figure 1 shows the dependence of the resonant electron density from θ_2 for different values of θ_1. From this figure one may conclude the resonant conditions could be satisfied only in a certain range of angles between the directions of the source HF1 and VLF waves and the geomagnetic field. Thus, we found the parameters of the sideband HF2 wave and suitable resonant electron density using a particular set of the parameters for the HF1 and VLF waves.

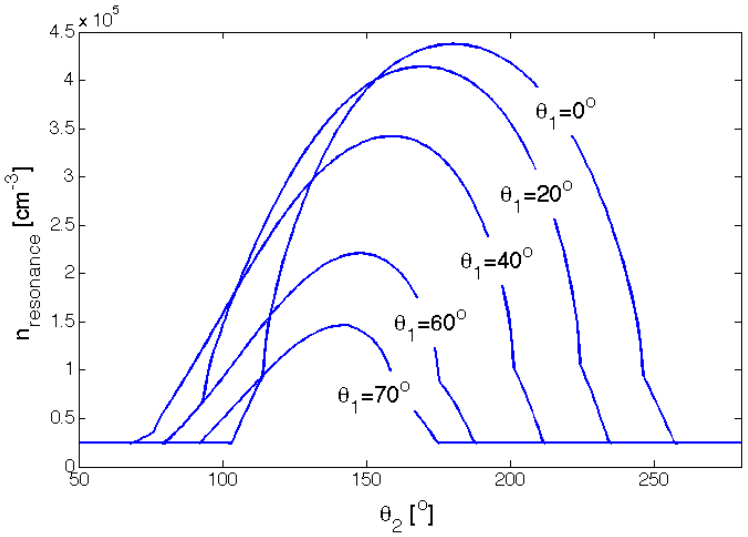

Figure 1: Dependence of the resonant electron density from θ_2 for different values of θ_1; geomagnetic field $B_0 = 0.5$.

III. Propagation of HF waves through magnetized plasma perturbed by VLF waves

In this section we use a FDTD technique [21] to simulate the propagation of HF waves through a magnetized plasma. Additionally, a section of the plasma density varies in time to mimic density perturbations due to VLF waves. Stability conditions which include a time varying density are not derived for this code, however the inverse VLF frequency and wavelength are much larger than the finite time step which satisfies the Courant Friedrichs Lewy limit [22]. Absorbing boundaries conditions were implemented as prescribed in [23].

As previously shown, the resonant condition can only be satisfied in a certain range of angles. Let us consider a 2D plane wave, HF1, propagating in the z-direction. In our simulation, the angles θ_1 and θ_2 are arbitrarily chosen within the range of allowable angles.The size of the 2D domain $L_x \times L_z$, is $L_x = 100l_{HF1}$ and $L_z = 150l_{HF1}$, where l_{HF1} is the wave length of HF1 wave. We suppose the ionosphere is homogeneous in the range ($0 \le x \le L_x : 0 \le z \le 6L_z/11$) while everywhere else includes VLF waves which produce the electron density variations. With the chosen set of values, the conditions (10) are satisfied if the electron density is $n_{e,res} = 3.5 \cdot 10^5 [cm^{-3}]$ which gives a corresponding electron plasma frequency of $\omega_{pe,res} = 3.33 \cdot 10^7 [rad/s]$.

The Interaction of VLF and HF1 waves may generate a sideband HF2. Using the dispersion relation for HF ordinary waves, we can find the wave vectors and wavelengths of the HF1, HF2 and VLF waves where

$$k_{HF1} = \sqrt{\omega_{HF1}^2 - \omega_{pe}^2} \tag{11}$$

$$k_{HF2} = \sqrt{\omega_{HF2}^2 - \omega_{pe}^2} \tag{12}$$

$$k_{||VLF} = (k_{HF1}\sin\theta_1 - k_{HF2}\sin\theta_2)\sin\theta_1 + (k_{HF1}\cos\theta_1 - k_{HF2}\cos\theta_2)\cos\theta_1 \tag{13}$$

$$k_{\perp VLF} = (k_{HF1}\sin\theta_1 - k_{HF2}\sin\theta_2)\cos\theta_1 + (k_{HF1}\cos\theta_1 - k_{HF2}\cos\theta_2)\sin\theta_1 \tag{14}$$

The simulation parameters for the HF_1, HF_2, VLF waves are given in Table 1 below.

Table 1: Simulation Parameters

θ_1	$20\pi/180\ [rad]$
θ_2	$135\pi/180\ [rad]$
k_{HF1}	$0.152\ [m^{-1}]$
k_{HF2}	$0.122\ [m^{-1}]$
k_{VLF}	$0.2320\ [m^{-1}]$
$k_{\|\|VLF}$	$0.2039\ [m^{-1}]$
$k_{\perp VLF}$	$0.1107\ [m^{-1}]$
k_{HF2}	$0.1220\ [m^{-1}]$
$k_{\|\|HF2}$	$-0.0516\ [m^{-1}]$
$k_{\perp HF2}$	$0.1106\ [m^{-1}]$

Thus, we expect to see the HF_2 wave propagating at angle $\theta_2 - \theta_1 = 115°$ relative to the HF_1 wave, which is positive in the *x*-direction and negative in the z-direction. The source of the HF_1 plane wave is given at position $z = L_z/2$ as

$$J_z(0 \le x \le L_x, z = L_z/2) = \frac{10^{-4}\sin(2\pi f_{HF1}t)}{3cosh(f_{HF1}(t - T/6)/8)} \tag{15}$$

Where $T = L_z/v_f$ is the total simulation is time and v_f is the phase velocity of HF_1 wave. The VLF produces variations in electron density with amplitude given by

$$dn_e(0 < x < L_x, 6L_z/11 < z < L_z) = \delta n_{e,res} \sin(\omega_{VLF} t - k_{\perp VLF} x - k_{||VLF} z) \quad (16)$$

where the amplitude is a small fraction of the averaged electron density, $\delta \leq 0.01$

The simulation results confirm the appearance of HF_2 waves. Figure 2 shows the spatial distribution of the absolute value of the electric field at time $t = 2T/3$ in the case when $\delta = 0.01$. The black vertical line in the middle of the figure depicts source position. The white vertical line divides the area with homogeneous ionosphere and the area with ionosphere disturbed by VLF waves. The source (15) creates two HF_1 wavetrains propagating in opposite directions. The wavetrain moving to the left is undisturbed. In contrast, the wavetrain moving to the right interacts with the VLF wave and generates the HF_2 wave propagating down and backward, leaving the area of perturbed ionosphere. The area inside the blue square includes a 'pure' HF_2 wave propagating at angle 115° relative to the direction of HF_1 wave. In the moment of time considered, the main body of HF_1 wavetrain is already far away from the white vertical line.

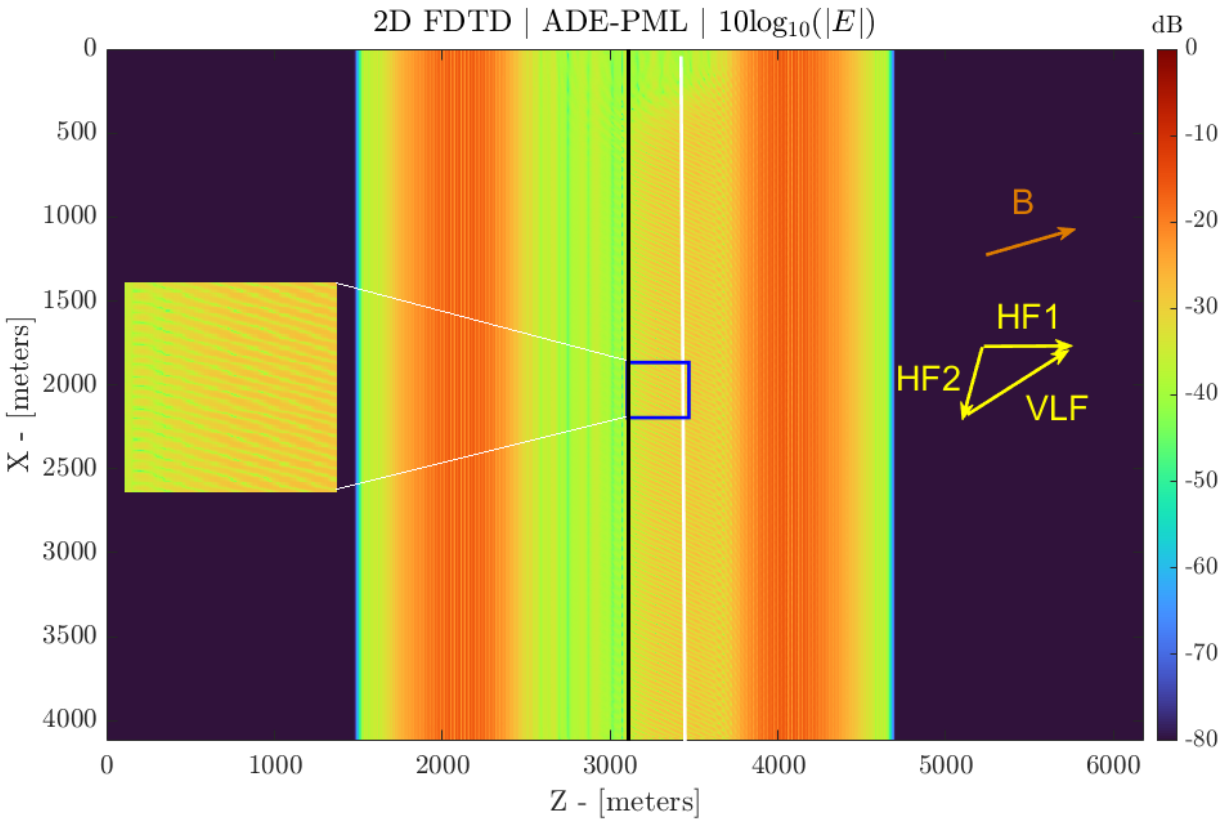

Figure 2. Spatial distribution of the electric field at time $t = 2T/3$.

Figure 3 displays the temporal variations of the electric field components at positions $z = 4L_y/11 + 3l_0$ and $z = 6L_y/11 - 3l_0$ placed symmetrically relative to the source position. Note, that both 'measurement' points are placed outside the area with VLF waves. The beginning of the curves on the left and right panels are similar. The rest of the curves are different, especially for the E_z component. The tails of the curves on the left panels exclusively represents the HF_2 wave. Indeed, the peak on the spectral density plot in Figure 4 equals ω_{HF2}. The spatial spectral density of E_y measured at time T along line $(0 \le x \le L_x, z = 6L_z/11 - 3l_{HF1})$ shows a peak at position $k = k_{\perp HF2}$ in Figure 5.

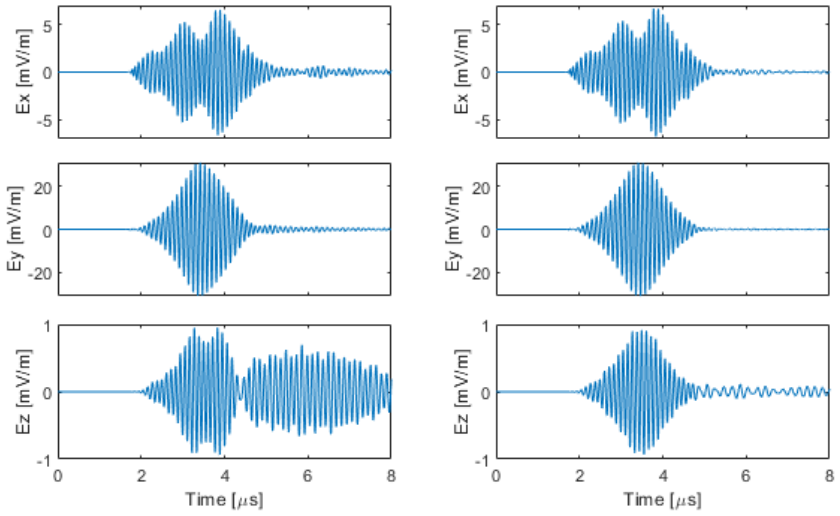

Figure 3. Left: Temporal variation of the electric field at positions $z = 6L_y/11 - 3l_0$. Right: $z = 4L_y/11 + 3l_0$

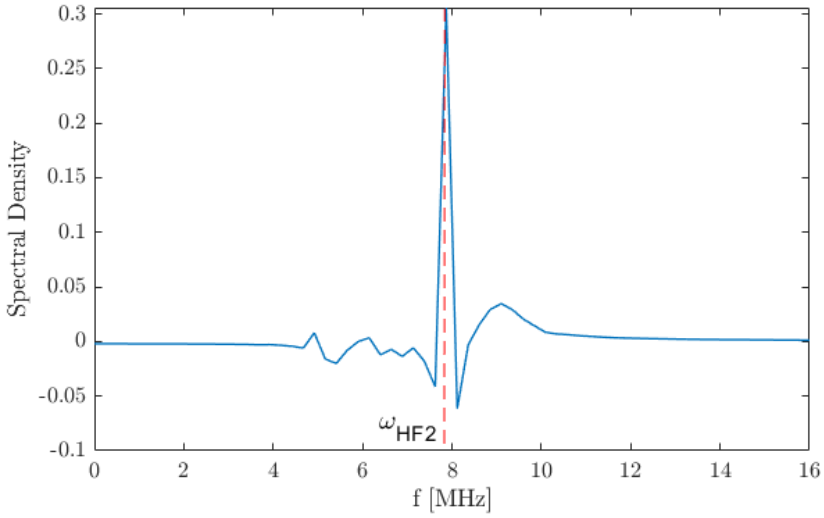

Figure 4. Spectral density of electric field E_z at position $z = 6L_y/11 - 3l_0$

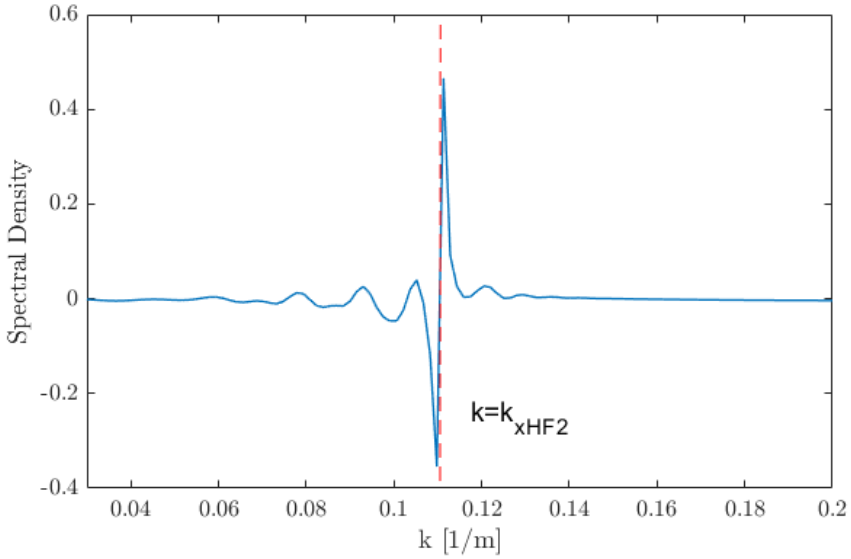

Figure 5. Spatial spectral density of $E_y(0 \le x \le L_x, z = 6L_z/11 - 3l_{HF1})$. The peak value equals $k_{\perp HF2}$.

As we can see from the Figures 2 and 3, the amplitude of the HF2 wave is about 3% of the amplitude of the original HF1 wave. Figure 6 shows the temporal variation of the electric field in case when the amplitude of the electron density variation is 0.01%. In this case the peak amplitude of HF2 wave is about 0.03% of the peak amplitude of the original HF1 wave.

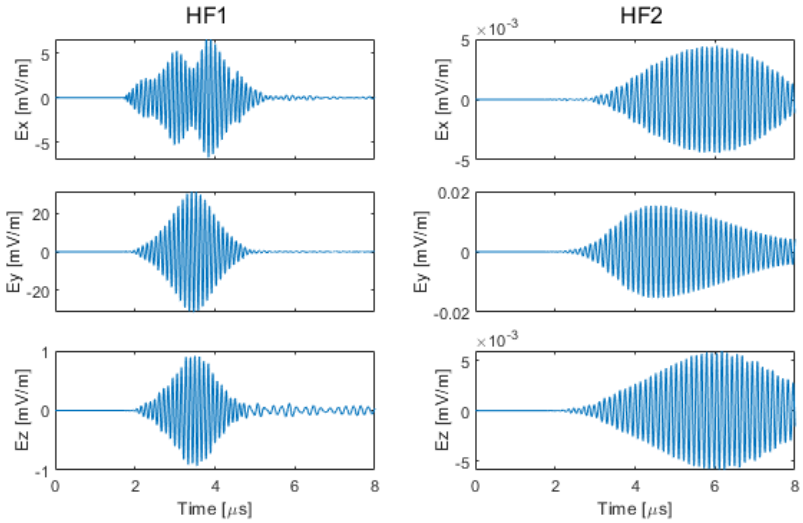

Figure 6. Left: temporal variation of the electric field at position $z = 6L_y/11 - 3l_0$. Right: difference between the electric fields at position $z = 6L_y/11 - 3l_0$ and at position $z = 4L_y/11 + 3l_0$ or the electric field of the HF2 wave. This simulation was implemented with amplitude of the electron density variations 0.01%.

IV. Conclusions

To the best of our knowledge, this is the first time the appearance of sideband HF waves are shown by the direct simulation of HF wave propagation through the ionosphere perturbed by VLF waves. The frequency of the sideband wave is the difference between the frequencies of the original HF and VLF waves. The wave vector components of sideband are also the difference between wave vector components of the original HF and VLF waves. The amplitude of the sideband is proportional to the intensity of VLF wave. Considering the examples shown above, the amplitude of HF sidebands is about 0.03% from the amplitude of the incident wave if the electron density variations due to the VLF wave is 0.01% from the averaged electron density. Simulations with parameters which do not satisfy resonance show no sideband generation.

This effect is possible only if the relations between parameters (frequencies and wave vectors) of HF and VLF waves are satisfy conditions (10). These conditions may be satisfied for the wide ranges of realistic ionosphere and VLF parameters. Another word it is not an exotic phenomenon but phenomena which should be seen on the regular basis almost always when HF wave propagates through the disturbed turbulent ionosphere. Although not shown, this effect is also applied for the interaction of HF and lower-hybrid waves.

FDTD technique for magnetized plasma has been used for computer simulations. The novelty introduces in our approach is a time-dependent property of the medium, i.e., the electron density of ionosphere plasma changes in time by propagating VLF wave.

REFERENCES

[1] Pedersen, T. R., M. McCarrick, E. Gerken, C. Selcher, D. Sentman, H. C. Carlson, and A. Gurevich, Magnetic zenith enhancement of HF radioinduced airglow production at HAARP, Geophys. Res. Lett., 30 (4), 1169, doi:10.1029/2002GL016096, 2003.

[2] Platino, M., U. S. Inan, T. F. Bell, J. Pickett, E. J. Kennedy, J. G. Trotignon, J. L. Rauch, and P. Canu (2004), Cluster observations of ELF/VLF signals generated by modulated heating of the lower ionosphere with the HAARP HF transmitter, Ann. Geophys., 22(7), 2643–2653, doi:10.5194/angeo-22-2643-2004.

[3] Papadopoulos, K., T. Wallace, G. M. Milikh, W. Peter, and M. McCarrick (2005), The magnetic response of the ionosphere to pulsed HF heating, Geophys. Res. Lett., 32, L13101, doi:10.1029/2005GL023185.

[4] Platino, M., U. S. Inan, T. F. Bell, M. Parrot, and E. J. Kennedy (2006), DEMETER observations of ELF waves injected with the HAARP HF transmitter, Geophys. Res. Lett., 33, L16101, doi:10.1029/2006GL026462.

[5] Piddyachiy, D., U. S. Inan, T. F. Bell, N. G. Lehtinen, and M. Parrot (2008), DEMETER observations of an intense upgoing column of ELF/VLF radiation excited by the HAARP HF heater, J. Geophys. Res., 113, A10308, doi:10.1029/2008JA013208.

[6] Eliasson, B., and K. Papadopoulos (2008), Numerical study of mode conversion between lower hybrid and whistler waves on short-scale density striations, J. Geophys. Res., 113, A09315, doi:10.1029/2008JA013261.

[7] Ganguli, G., L. Rudakov, W. Scales, J. Wang, and M. Mithaiwala. Three-dimensional character of whistler turbulence. Physics of Plasmas, 17 (5), article id. 052310 8 pp. (2010).

[8] Kuo,S.,A. Snyder, P.Kossey,C.-L.Chang, and J. Labenski (2011), VLF wave generation by beating of two HF waves in the ionosphere, Geophys. Res. Lett., 38, L10608, doi:10.1029/2011GL047514.

[9] Cohen, M. B., and M. Golkowski (2013), 100 days of ELF/VLF generation via HF heating with HAARP, J. Geophys. Res. Space Physics, 118,6597– 6607, doi:10.1002/jgra.50558.

[10] Vartanyan, A., G. M. Milikh,B. Eliasson, A. C. Najmi, M. Parrot,and K. Papadopoulos (2016), Generation of whistler waves by continuous HF heating of the upper ionosphere, Radio Sci., 51, 1188– 1198,doi:10.1002/2015RS005892

[11] Kuo, S., & Lee, M. C. (2017). On the VLF wave generation by beating of two HF heaters. *Physics of Plasmas*, *24*(2), [022902]. https://doi.org/10.1063/1.4976123

[12] N. Borisov, Excitation of VLF perturbations in the F-region of the ionosphere by beating HF O-mode waves Phys. Plasmas **27**, 012101 (2020); https://doi.org/10.1063/1.5119514

[13] Alpert Y. I. and I. P. Pitaevskii, “Scattering of electromagnetic waves by inhomogeneities excited in a plasma by a rapidly moving body,” AIAA J., 1, 4, 1001–1009, 1963.

[14] Mitchell Jr. F. H., W. R. Mahaffey, and R. F. Jacob, Modeling plasma effects on radar cross section of reentry vehicles, IBM J. Res. Develop., 13, 4, 468–474, 1969.

[15] Lin T. C. and L. K. Sproul, Influence of reentry turbulent plasma fluctuation on EM wave propagation, Comput. Fluids, 35, 7, 703–714, 2006.

[16] Hartunian R. A., G. E. Stewart, S. D. Fergason, T. J. Curtiss, and R.W. Seibold, Causes and mitigation of radio frequency blackout during reentry of reusable launch vehicles, Aerosp. Corporation, El Segundo, CA, Aerosp. Rep. ATR-2007(5309)-1, 2007.

[17] Sotnikov, V. I., V. Fiala, F. Lefeuvre, D. Lagoutte, and M. Mogilevsky (1991) Excitation of sidebands due to nonlinear coupling between a VLF transmitter signal and a natural ELF emission, J. Geophys. Res.96, A7, 11363-2156-69

[18] Sotnikov, V. I., D. Schriver, M. Ashour-Abdalla, and J. Ernstmeyer (1994) Excitation of sideband emissions by a modulated electron beam during the CHARGE 2B Mission, J. Geophys. Res.99, A5, 8917-23

[19] Sotnikov V. I., J. N. Leboeuf, and S. Mudaliar Scattering of Electromagnetic Waves in the Presence of Wave Turbulence Excited by a Flow with Velocity Shear, *IEEE Trans. Plasma Sci.*, vol. 38, no. 9, pp. 2208–2218, 2010

[20] Yee, K. Numerical solution of initial boundary value problems involving Maxwell's equations in isotropic media, IEEE *Trans. Antennas Propag.*, vol. AP-14, no. 3, pp. 302–307, May 1966.

[21] S. Pokhrel, V. Shankar, and J. J. Simpson. 3-D FDTD Modeling of Electromagnetic Wave Propagation in Magnetized Plasma Requiring Singular Updates to the Current Density Equation. *IEEE Trans. Antennas Propag* , vol. 66, no. 9, pp. 4772-81, 2018

[22] A. Taflove and S. C. Hagness, *Computational Electrodynamics: The Finite-Difference Time-Domain Method*, 3rd ed. Norwood, MA, USA: Artech House, 2005.

[23] Gedney S. D. and B. Zhao, An Auxiliary Differential Equation Formulation for the Complex-Frequency Shifted PML, IEEE Transactions on Antennas and Propagation, pp. vol. 58, no. 3, pp. 838-847, March 2010, doi: 10.1109/TAP.2009.2037765.